ingegneria sismica
International Journal of Earthquake Engineering
Anno XLIII - Num. 2 - 2026

Research on intelligent assessment and exercise risk prediction model of knee joint function in elderly patients

Xinghai Yang[1,2], *Xiaoyan Liu*[1,2,*], *Ye Li*[1,2] *and Xiaolu Zhang*[1,2]

[1] Department of Orthopedics, West China Hospital, Sichuan University, Chengdu 610041, China
[2] West China School of Nursing, Sichuan University, Chengdu 610041, China

SUMMARY: *This paper proposes a computational modeling oriented framework for intelligent knee function assessment and movement risk prediction in elderly patients. The framework revolves around the joint modeling of gait video, inertial signals, plantar pressure sequences, and knee flexion and extension measurements, and no longer relies on single source observations. This study constructs a data set containing 1240 evaluation samples from 186 elderly patients, and integrates multi-modal feature fusion, temporal representation of functional status and probabilistic risk inference mechanism in a unified framework to characterize the changes in joint stability, mobility and motor coordination. The experimental results show that the mean absolute error of functional score estimation is 4.9%, the accuracy of risk prediction is 91.3%, and the precision, recall and F1-score are 92.1%, 89.4% and 90.7%, respectively. Compared with CNN-LSTM, random forest and unimodal baseline models, the proposed framework shows strong stability and robustness under complex continuous action clips of elderly patients, which can provide feasible technical support for digital rehabilitation assessment and risk early warning in intelligent medical scenarios.*

KEYWORDS: *Multimodal fusion; Functional assessment; Temporal modeling; Risk prediction*

1 Introduction

As the aging of the population continues to deepen, knee joint functional degeneration has become an important factor affecting the independent mobility of the elderly. A large number of gait videos, inertial sensing signals, plantar pressure sequences and joint range of motion records have been accumulated in outpatient follow-up, rehabilitation training and home monitoring. These data provide the basis for the digital assessment of knee joint function, and also put forward higher requirements for the representation ability, cross-modal alignment ability and timing inference ability of the computational model. Traditional clinical assessment relies on scale scoring, manual observation and local index comparison, which can complete basic screening, but it is difficult to stably describe joint stability, load transfer characteristics and risk changes in continuous movements. Around this application scenario, establishing a computational framework that fuses multi-source perception, state estimation and risk prediction has become an important direction in the research of intelligent rehabilitation assessment.

This study focuses on two quantifiable goals. Firstly, the representation bias in the knee

*lxy711010@163.com
https://doi.org/10.65102/is2026569 Published: 30 April, 2026

joint function assessment of elderly patients is reduced by multi-modal feature fusion, and the recognition ability of gait abnormalities, flexion and extension limitation and load imbalance is enhanced. The second is to improve the accuracy of motion risk prediction through time series state modeling, so that the model can identify potential dangerous patterns in continuous action clips and output explanatory risk results. This setting is not limited to static classification, but emphasizes the dynamic evolution process of recovering knee functional status from heterogeneous data, which provides a computable basis for subsequent digital rehabilitation decision-making.

In related studies, Ben Hassine S et al. studied the classification method of unlabeled knee osteoarthritis based on gait videos, indicating that the combination of visual features and machine learning can support knee joint state recognition [1]. Xie J et al. proposed a functional monitoring scheme based on multi-dimensional plantar pressure characteristics, which proved that wearable pressure data had a strong representation value for knee joint function changes [2]. Li G et al. studied the relationship between dynamic plantar pressure changes and imaging manifestations of knee osteoarthritis, indicating that machine learning can be used to mine implicit load distribution patterns [3]. Raza A et al. proposed a gait classification method based on shoe-embedded inertial measurement unit, showing that inertial signals have good sensitivity in the discrimination of patient motion states [4]. Armstrong K et al. studied the application of markerless human motion analysis system in biometric identification of knee disorders, which provided a basis for extracting high-value functional indicators from motion trajectories [5]. Zhao Z et al. proposed a self-assessment method of sitting and standing test combined with computer vision, which expanded the technical path of knee joint function assessment at home [6]. Maiora J et al. studied the deep learning prediction method of fall risk for the elderly based on TUG test data, indicating that continuous action data can be used for risk judgment [7]. Lim Z K et al. proposed a machine learning risk prediction method combined with temporal gait features, which further showed that temporal features play a decisive role in the safety assessment of elderly sports [8].

Existing research has formed a pattern of parallel development of visual analysis, wearable perception and machine learning recognition. However, there are still some problems between different modalities, such as inconsistent sampling granularity, insufficient temporal correlation and weak unified representation, which leads to the fact that knee joint function assessment and risk prediction are often carried out separately, and it is difficult to form an integrated calculation chain. Based on this, this study constructs an intelligent knee function assessment and motion risk prediction model for elderly patients, which integrates multi-modal feature fusion, functional state time series representation and probabilistic risk inference mechanism in a unified framework, so that the assessment results and risk output share the same state space. The design not only strengthens the adaptation ability of the model to complex action clips, but also enhances the stability and landing of the evaluation results in intelligent medical scenarios.

2 Literature Review

2.1 Development and current situation of knee function assessment technology in elderly patients

Knee function assessment in elderly patients has gradually shifted from single point measurement to continuous data-driven analysis. Early assessment mostly relies on joint range of motion scale, manual gait observation and image reading, which can complete the basic classification, but it is difficult to stably describe weight transfer, flexion and extension

coordination and small compensatory movements. With the continuous expansion of data acquisition methods in rehabilitation monitoring scenarios, knee joint function assessment has begun to have obvious computational modeling characteristics, and the research focus has shifted from static interpretation to digital expression of continuous motion process.

Nishiyama et al. studied fall risk classification of the elderly based on single gait cycle data and machine learning, indicating that short-time motion segments can also form high discrimination after fine feature extraction [9]. Gonzalez-Castro et al. systematically reviewed the application of artificial intelligence in fall risk assessment, and pointed out that deep learning, traditional machine learning and wearable perception are jointly promoting the automation of risk assessment [10]. Wipperman et al. studied knee disease recognition and gait feature extraction based on digital wearable insoles, and proved that plantar pressure and gait signature can be used as important inputs for the calculation and representation of knee states [11]. Xu et al. studied an assistive device for rehabilitation monitoring of movement disorders combined with multi-sensor analysis and deep learning, indicating that heterogeneous sensory data can support continuous functional assessment after unified modeling [12].

These studies have promoted the knee joint function assessment from empirical judgment to computational description. However, at this stage, the use of single-modal features and local index analysis are still the main methods, and there is still a lack of unified expression for common motion retardation, balance compensation and load imbalance in elderly patients. For technical journal writing, knee function assessment is more suitable to be regarded as a multi-source time series calculation task, whose core is not only to obtain a certain value, but to establish a stable mapping between video, inertia, pressure and Angle data, so as to form a repeatable, comparable, and deployable intelligent evaluation mechanism.

From the perspective of technology evolution, the current methods have formed three main routes: visual perception, wearable sensing and cross-modal fusion. The visual route emphasizes the reconstruction accuracy of posture key points, joint angles and motion trajectories, which is suitable for home and outpatient scenes. The wearable route emphasizes signal continuity and quantitative sensitivity, which is suitable for capturing step frequency changes, support phase shifts and peak pressure abnormalities. The cross-modal route is oriented to model robustness, keeping the evaluation results consistent under different sampling frequencies and noise conditions. If intelligent assessment of knee function in elderly patients is to have real application value, it needs to continue to refine feature standardization, modal alignment and individual difference modeling, which also constitutes the technical basis for subsequent model design.

2.2 Research status and existing problems of sports risk prediction models

Exercise risk prediction plays a prospective judgment role in the knee joint assessment system of elderly patients. Its goal is not to repeat the existing state, but to identify potential instability trends based on continuous motion signals. Existing research has shifted from empirical rules to data learning, but the model design is still obviously affected by the way of sample organization, the way of risk definition and the boundary of scenarios. For elderly patients, the risk is not only represented by the single outcome of fall, but also involves multi-level manifestations such as gait disorder, joint instability, abnormal load and deviation of rehabilitation action execution. Therefore, the prediction model needs stronger state discrimination ability.

Shen et al. proposed a wearable knee rehabilitation system based on graphene textile composite sensors, which verified the stable collection ability of flexible sensors for changes

in joint activities at the implementation level [13]. Hu et al. studied HGcnMLP, a markerless 3D pose estimation method based on monocular video of smartphone, and showed that low-cost visual acquisition can also form an effective assessment link for patients with musculoskeletal diseases [14]. Cedeno-Moreno et al. proposed a computer vision system based on gait feature analysis for fall risk assessment in the elderly, showing that visual gait parameters have a stable contribution to risk determination [15]. Feng et al. reviewed the application progress of wearable sensors in gait analysis after total knee replacement, indicating that gait fluctuations during postoperative recovery can provide a continuous observation basis for risk identification [16].

These results show that exercise risk prediction has shifted from single index threshold judgment to sequential pattern learning. However, most of the existing models are based on fall classification, postoperative recovery monitoring or general gait abnormality recognition, and the coupling with the functional status of the knee joint in elderly patients is still not sufficient. In terms of computational modeling, risk prediction should deal with at least three kinds of information at the same time. One is the temporal structure such as gait rhythm, support time and swing transition. One is the functional cues such as knee flexion and extension range, valgus deviation and center of gravity migration. One is the cross-modal consistency from video, pressure, and inertial signals.

If the model only relies on a single time window or isolated statistics, the output results often reflect local anomalies, but it is difficult to accurately describe the risk accumulation process in continuous actions. Therefore, the motion risk prediction for elderly patients is more suitable to adopt a state-driven sequential learning path, so that the function assessment results and risk inference results share a unified representation basis, so as to improve the stability, interpretability and scene adaptability of the prediction results. From the perspective of application, outpatient screening pays more attention to rapid identification, rehabilitation follow-up emphasizes change trends, and home early warning relies more on low-cost real-time inference. The corresponding computational requirements of the three scenarios are not the same, which requires the model to consider lightweight deployment, noise immunity and cross-crowd migration performance in addition to accuracy.

2.3 Analysis of intelligent assessment and risk prediction technology

The core of intelligent assessment and risk prediction technology analysis is to convert scattered motion observations into computable and comparable state representations, and then complete the assessment output and risk inference by a unified model. For the knee joint scene of elderly patients, this technical process involves not only the acquisition of action information, but also the time alignment between multi-source data, the continuous coding of functional status, and the probabilistic expression of risk levels. Only when the evaluation and prediction are put into the same calculation chain, the model can maintain the stability of state identification and the continuity of risk output at the same time.

Gianzina et al. studied the assessment of gait recovery based on wearable inertial sensors after total knee replacement, indicating that continuous inertial signals are suitable for describing dynamic fluctuations in the recovery phase [17]. Ceballos-Laita et al. proposed the application of genu valgum Angle assessment based on computer vision, and verified the effectiveness and consistency of mobile vision tools in Angle measurement [18]. Talaa et al. studied the automatic monitoring method of gait rehabilitation for home scenes, and pointed out that visual analysis has high practicability in remote rehabilitation evaluation [19]. Horsak et al. verified the parallel effectiveness of marker-free motion capture on smartphones to quantify lower limb kinematic parameters, indicating that low-threshold acquisition devices

can support pathological gait analysis [20]. Iovanel et al. studied the role of wearable technology in outcome measurement and support after joint replacement, emphasizing the important value of continuous tracking for patient recovery evaluation [21].

In order to more clearly compare the data sources, technical paths of current intelligent assessment and risk prediction methods and their inspiration for the research in this paper, the existing representative studies can be summarized as follows, as shown in Table 1.

Table 1: Comparison of intelligent assessment and risk prediction technology routes

Study	Data Source	Technical Path	Inspiration for This Study
Gianzina et al. [17]	Inertial sensor gait data	Quantification of the postoperative recovery process	Strengthens continuous state tracking
Ceballos-Laita et al. [18]	Visual angle measurement data	Computer vision-based assessment	Supports low-cost angle analysis
Talaa et al. [19]	Home gait videos	Remote automatic monitoring	Supports home-based assessment deployment
Horsak et al. [20]	Markerless smartphone videos	Quantification of lower-limb kinematics	Improves the convenience of data acquisition
Iovanel et al. [21]	Wearable recovery follow-up data	Outcome measurement and continuous support	Strengthens long-term dynamic observation

It can be seen from Table 1 that the current technology has covered multiple directions such as visual measurement, wearable perception, home monitoring and mobile terminal acquisition, but there are still few integrated frameworks for intelligent assessment of knee function and movement risk prediction in elderly patients. A more feasible path should be to establish the temporal representation of functional states on the basis of multi-modal feature fusion, and then send the assessment results to the probabilistic risk prediction layer to realize the collaborative output of assessment and early warning. Such a technical organization method is not only in line with the hierarchical modeling logic of computer models, but also more suitable for the real-time, continuity and deployability requirements of intelligent medical scenarios.

At the same time, the model should also have the ability of missing mode compensation, cross-device normalization and individual threshold adaptation to avoid assessment deviation caused by sampling environment changes, and ensure the consistency of risk output in outpatient, rehabilitation and home scenarios. This is also the direct logical basis for this paper to turn to the design of integrated model after the survey.

3 Intelligent knee function assessment and exercise risk prediction model for elderly patients

3.1 Intelligent assessment model of knee joint function

In order to ensure that the subsequent multi-modal fusion, temporal state representation and risk inference are established on a unified computing basis, this paper first constructs an intelligent assessment model for knee joint function. For the knee function monitoring scenario of elderly patients, the gait video frame sequence, plantar pressure matrix, inertial

measurement unit signal and knee flexion and extension Angle time stream are organized as a unified input. The four types of data were synchronously sliced under the patient-level index, and constituted a multi-modal sample unit according to a fixed-length window. The visual branch mainly extracted the topology of key points of the lower limbs, the change of the trajectory around the knee and the transfer of the center of gravity. The process of load distribution and pressure redistribution of the front and rear palm in the recovery support phase of the pressure branch; The inertial branch encodes tibial-femoral relative rotation, step frequency disturbance and angular velocity fluctuation. The Angle branch directly describes the range of flexion and extension, the range of motion and the symmetry of action. The extracted results of each branch are not directly used for isolated discrimination, but scale alignment and semantic mapping are completed in the shared embedding space, so that different modalities enter the same functional state representation framework while maintaining their own discrimination ability.

In the scenario of elderly patients, knee joint function assessment should not only reflect the joint activity itself, but also reveal the stability, coordination and compensation trends during action execution. To this end, this paper uses a dual-task structure to organize the evaluation output, so that the model generates continuous function scores and functional status grades simultaneously. The continuous score was used to describe the patient's comprehensive level of flexion and extension control, load transfer, gait rhythm and support stability, which was suitable for tracking subtle changes in the rehabilitation process. Status levels are used to form discrete discriminant results oriented to outpatient screening, rehabilitation stratification, and training adjustment. The dual-task parallel modeling can reduce the information compression brought by the single output head, so that the evaluation results are not only continuous, but also retain clear state boundaries.

In order to more clearly illustrate the connection relationship between input organization, feature extraction and functional output, the overall evaluation process is drawn as a structural schematic, as shown in Fig. 1.

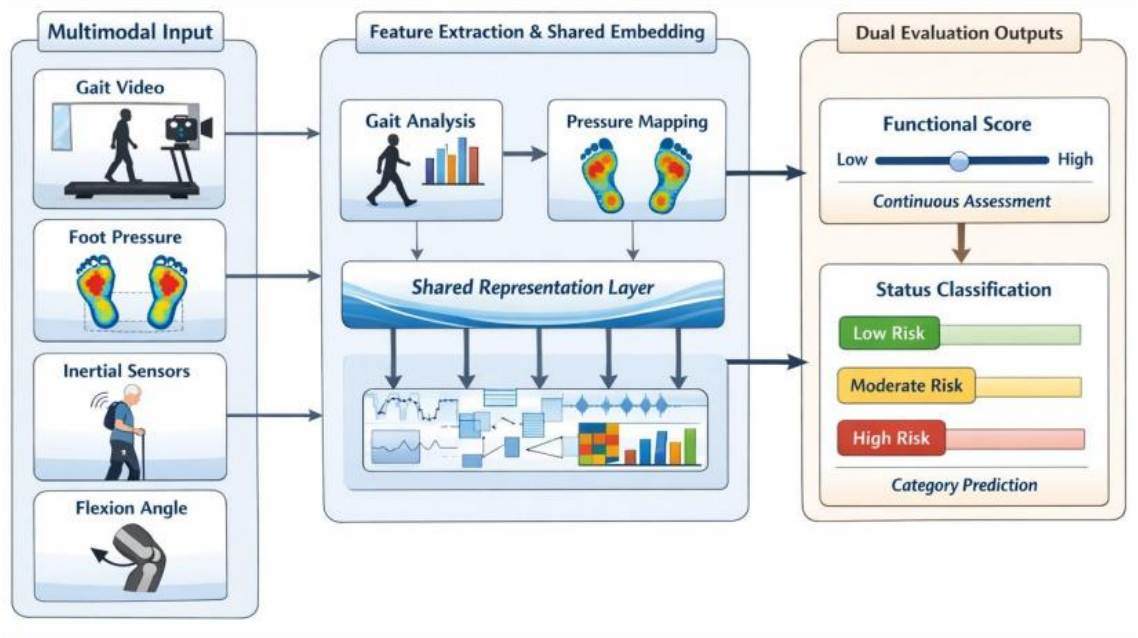

Figure 1: The overall flow chart of the intelligent assessment model for knee function

Fig. 1 illustrates the complete path from the patient-level multimodal input to the shared representation layer to the continuous functional score versus state-level output. The left is the

original acquisition layer, the middle is the parallel feature extraction and shared embedding layer, and the right is the dual-task evaluation output head. This flow unifies gait video, plantar pressure, inertial signals, and flexion and extension Angle measurements into the same computational chain, enabling the model to simultaneously output continuous functional scores and state categories. The continuous score is suitable for describing the subtle changes in the progress of rehabilitation, and the status category is suitable for outpatient screening and hierarchical judgment. With the combination of the two results, knee function assessment can be extended from single observation to quantitative analysis oriented to dynamic process.

At the implementation level, the backbone evaluation network adopts a series structure of two-layer 3D convolution and bidirectional gated recurrent unit. The convolutional layer is responsible for capturing the local dynamic texture and spatial geometry in a short time window, and the bidirectional gating unit is responsible for aggregating the trend difference between the two stages before and after the same action cycle. A shared embedding layer is set in the tail to compress the visual, pressure, inertia and Angle information into a unified functional state vector. The vector inputs both the continuous scoring head and the state label discrimination head, and maintains the semantic coordination of the two types of outputs by consistency constraints. Such a design enables the model to no longer rely on the individual strengths of one modality, but to form a stable computational representation for knee function in elderly patients through joint training. Considering the slow movement speed of elderly patients, large differences in action completion, and missing sampling in some samples, parameter sharing and inter-layer normalization strategies are used in the network to reduce the disturbance of individual differences on state expression.

3.2 Multimodal feature fusion component of knee joint

The multimodal feature fusion component of the knee joint plays a key role in connecting the raw sensory data with the upper-level state modeling. The video, pressure, inertia and Angle data in the knee joint monitoring scene of elderly patients have not only differences in physical dimension, but also differences in sampling frequency, noise pattern and loss form. If the original features are directly spliced, the visual texture features will dominate the expression due to the high dimension, and the local anomalies in the pressure and inertia modes are easy to be weakened. Therefore, this paper adopts a multi-stage fusion process of "normalized mapping-quality assessment-weight assignment-shared aggregation" to recover the correspondence between different modalities in the shared embedding space, so that the fusion results not only retain local abnormal information, but also maintain the stability of the overall functional expression.

In order to obtain a consistent statistical distribution of the original features under different sampling scales in the shared space, this paper first performs parametric normalization and linear projection on the single-modal coding results, and the calculation form is shown in the following equation.

$$z_m = W_m \cdot LN\left(\frac{x_m - \mu_m}{\sigma_m + \varepsilon}\right) + b_m \tag{1}$$

where x_m represents the original encoding vector of the m modality, μ_m and σ_m represent the mean and standard deviation obtained by the statistics of the modality in the training phase, $LN(\cdot)$ represents the layer normalization operation, W_m and b_m are the learnable projection parameters, and z_m is the modal representation after entering the shared space. Firstly, the natural differences between different modalities in dimension and scale are eliminated by standardization, and then they are mapped into the shared feature domain of the

same dimension by linear projection. After this process, the posture structure from the gait video, the load fluctuation from the plantar pressure matrix, the angular velocity change from the inertial signal, and the activity amplitude from the flexion and extension Angle time flow can be compared in the same coordinate system, which lays the foundation for the subsequent weight allocation and unified aggregation.

In order to avoid a certain noise mode occupying too high weight in the fusion stage, this paper further introduces the modal reliability allocation mechanism, whose weight is calculated as shown in the following equation.

$$\alpha_m = \frac{\exp(q^\top \tanh(Uz_m + Vc_m))}{\sum_{k=1}^{M} \exp(q^\top \tanh(Uz_k + Vc_k))} \tag{2}$$

Here, α_m is the reliability weight of the m mode, c_m represents the quality description vector composed of sampling completeness, signal smoothness and missing rate, and q, U, V are the learnable parameter matrices. This formula takes "feature content" and "data quality" into the weight estimation process at the same time. If the video key points are occluded seriously, the local channel distortion of the pressure pad or the inertial signal drift in a certain time window, the credibility of the corresponding mode will automatically decrease. In this way, the fusion stage will not cause the overall shift due to the local anomaly of one input source, and the model can maintain a relatively stable output under different sampling conditions.

In order to illustrate the mapping and weight assignment process of multimodal inputs in the unified space, the data streams before and after fusion are organized as structural schemata in this paper, as shown in Fig. 2.

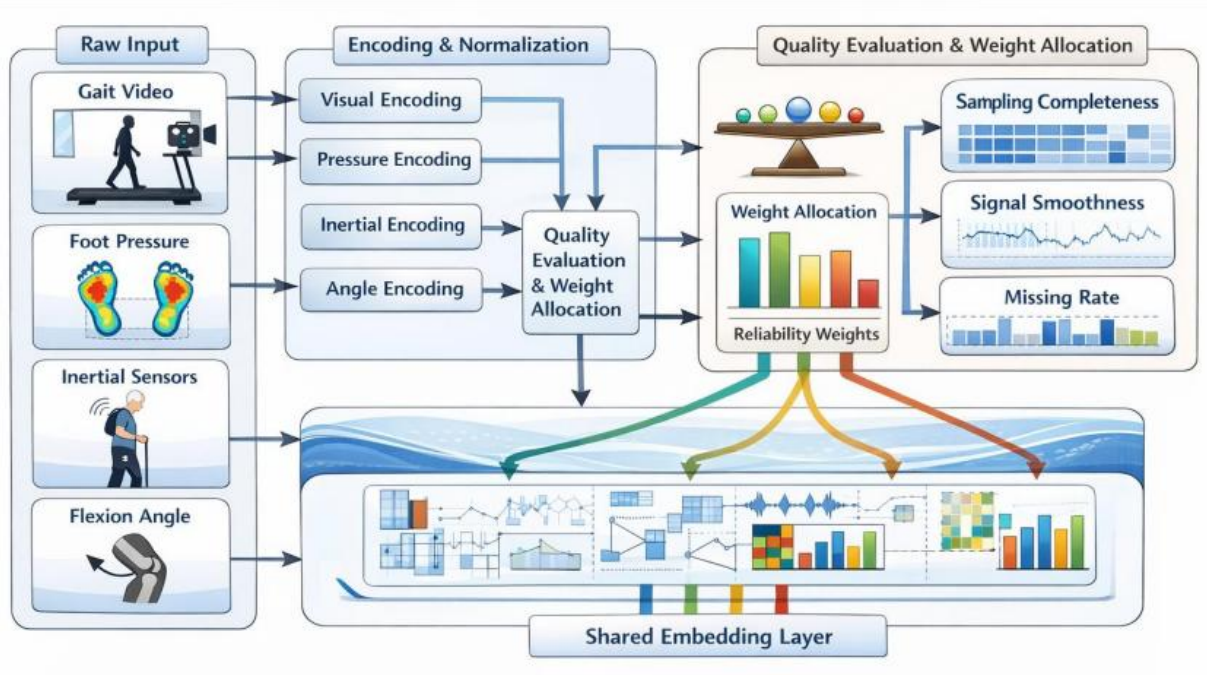

Figure 2: Structure diagram of multi-modal input alignment and confidence assignment

Fig. 2 illustrates the process of four types of raw inputs entering the shared space after coding normalization, quality assessment, and weight assignment. The vision, pressure, inertia and Angle data first form a single-modal representation respectively, and then combine the sampling integrity, signal smoothness and missing rate to complete the confidence estimation,

and then enter the shared embedding layer. This process can dynamically adjust the contribution ratio according to the data quality of different modalities, thereby reducing the impact of occlusion, drift and incomplete sampling on the fusion results. For the elderly patient scenario, this structure helps to maintain the output stability of the model across different device conditions and sampling environments.

In order to further combine the weighted modal representations into a fusion vector with the ability of structure awareness, the following aggregation expression is used in this paper.

$$h = \sum_{m=1}^{M} \alpha_m \odot z_m + \lambda\left(A_p p + A_i i\right) \tag{3}$$

Here, h is the shared state vector after fusion, $\odot$ represents elemon-wise weighting, p and i represent the structural hint term of pressure prior and inertia prior respectively,A_p and A_i are the corresponding projection matrices, and λ is the prior injection strength. On the basis of weighted aggregation, this formula introduces a structural prior closely related to the knee joint function, so that the fusion result not only retains the information in the statistical average sense, but also can explicitly strengthen the key patterns such as load redistribution of the front and rear hand, lateral displacement of the support phase, and rotation constraints.

In order to maintain a consistent geometric relationship between the fusion results across different modalities, this paper continues to add the cross-modal consistency loss, which has the form shown in the following equation.

$$\mathcal{L}_{con} = \|S_v - S_p\|_F^2 + \|S_v - S_i\|_F^2 + \|S_p - S_a\|_F^2 \tag{4}$$

Here, S_v, S_p, S_i and S_a represent the similarity matrices of vision, pressure, inertia and Angle modes in the shared space, respectively. The loss does not require that the modal values are completely consistent, but that they maintain coordination in the sample relationship structure. If two patients are close in visual gait performance, they should also show similar adjacency relationship in pressure and inertial response. With this structure-level constraint, the fusion layer can reduce the distortion of the overall representation by single-modal noise and improve the stability of the state comparison between patients.

After processing by the fusion layer, the video, pressure, inertia and Angle information are compressed into a comparable, alignable and noise resistant shared vector, which provides a stable input for continuous state representation and improves the adaptability of the whole model in the face of heterogeneous data.

3.3 Time series representation component of knee functional state

The task of the time series representation component of knee function state is to extend the static shared vector obtained by the fusion layer to a continuous state trajectory. The changes of knee joint function in elderly patients are often manifested in the pre-and post-action stages, not limited to an isolated moment. The center of gravity drift, flexion and extension delay, and support deviation during the stand up, sit down, gait transition, and return to normal phases need to be placed on a time continuum to be accurately interpreted. Based on this feature, in this paper, a fixed-length window and overlapping step size are used to slice the fusion vector sequence, so that the model can establish a balanced representation between short-time fluctuations and inter-cycle trends.

In order to let the time series input enter the state representation layer under unified rules, this paper first defines the construction mode of overlapping window, and its form is shown in

the following equation.

$$X_t = [h_{t-L+1}, h_{t-L+2}, \ldots, h_t], \quad \Delta = \frac{L}{2} \tag{5}$$

Here, h_t represents the fusion vector at time t, L is the time window length and Δ is the step size. This formula organizes adjacent state segments by overlapping Windows to ensure that the context information will not be lost due to time segmentation in the action transition phase. For the knee joint evaluation of elderly patients, many abnormalities are not directly determined by a single frame, but are accumulated by changes in a continuous movement. The window overlap strategy enables the model to repeatedly observe the same critical stage in multiple local segments, thereby improving the perception of gait instability, delayed center of gravity transfer, and limited flexion and extension.

In order to depict the balance relationship between short-time transition and smooth maintenance inside the window, this paper constructs a gated state update mechanism, which is specifically expressed as follows.

$$s_t = g_t \odot \phi(W_x h_t + W_s s_{t-1}) + (1 - g_t) \odot s_{t-1} \tag{6}$$

where s_t is the state vector at time t, g_t is the gating coefficient, $\phi(\cdot)$ is the nonlinear mapping, and W_x and W_s are the learnable parameters. This formula takes into account both the correction effect of current input and the retention effect of historical state. When there is a significant increase in genu valgum, a delay in the support phase or a shift in the pressure peak at a certain time period, the gating coefficient will amplify the influence of the current fusion vector on the state. When the state change is gentle, the historical information takes a higher proportion, so as to maintain the smoothness of the sequence. Such a design enables the temporal representation to capture sudden anomalies without violent oscillations due to local noise.

In order to illustrate the flow mode of the timing window in the process of state propagation, the dynamic propagation structure is shown in Fig. 3.

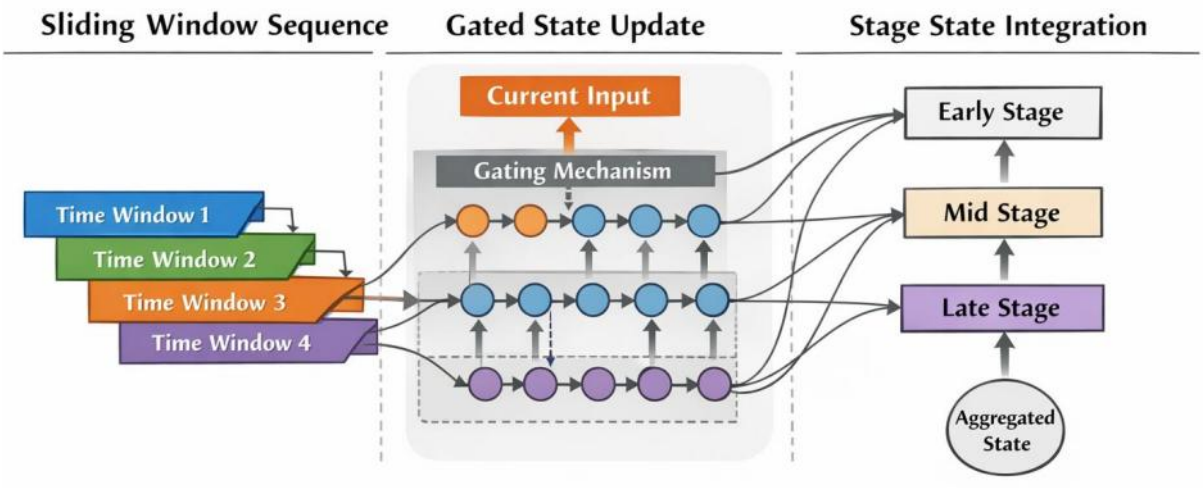

Figure 3: Time series propagation diagram of knee functional status

Fig. 3 depicts how overlapping time Windows flow in the state propagation layer. The left is a sequence of continuous Windows split by a fixed length, the middle is the gated state update layer, and the right is the stage state aggregation layer. The model refers to both the

current input and the historical state at each time step, thus preserving the continuous relationship between the previous and subsequent stages during the action. For the knee joint scene of elderly patients, this propagation structure can more fully describe the dynamic changes such as support transition delay, stride contraction and load offset, making the state representation closer to the real motion process.

In order to enhance the model's ability to focus on key stages, this paper introduces stage-aware attention on the state sequence, and its weight is calculated as shown in the following equation.

$$\beta_t = \frac{\exp(u^\top \tanh(W_b s_t + r_t))}{\sum_{\tau=1}^{L} \exp(u^\top \tanh(W_b s_\tau + r_\tau))} \tag{7}$$

Here, β_t is the phase weight at the t time step, r_t represents the action phase encoding vector, and u and W_b are the learnable parameters. This formula takes the time position and motion phase into the weight estimation simultaneously, so that the model will not deal with all segments equally, but pay more attention to the most sensitive parts of the knee joint function, such as the support transition, the peak of flexion and extension, the initial step of the lift and the return phase. Stage attention makes the state trajectory more selective, especially suitable for scenes with uneven action rhythms and large local stage differences in elderly patients.

In order to further transform the state sequence into a continuous index with interpretability, this paper defines the knee functional stability index as follows.

$$\kappa_t = \eta_1 \|\Delta\theta_t\|_2 + \eta_2 \|\Delta p_t\|_2 + \eta_3 \|\Delta a_t\|_2 \tag{8}$$

Here, $\Delta\theta_t$ represents the flexion and extension Angle change at adjacent moments, Δp_t represents the pressure distribution change, Δa_t represents the inertial response change, and η_1 to η_3 are the weight coefficients. This formula compresses the dynamic changes of three sources of Angle, pressure and inertia into a unified stability index, which is used to describe the fluctuation degree of joint state in continuous action. When κt continues to rise, it indicates that the patient has a clear trend of instability when completing the action, and this indicator will also be directly used as an important input for subsequent risk prediction.

In order to further constrain the smoothness and discrimination of sequence representation in adjacent Windows, this paper adds the loss function of time series representation. The specific form is shown in the following equation.

$$\mathcal{L}_{tem} = \sum_{t=2}^{L} \| s_t - s_{t-1} \|_2^2 + \rho \sum_{(i,j)} y_{ij} \|\bar{s}_i - \bar{s}_j\|_2^2 \tag{9}$$

Here, $\sum_{t=2}^{L} \| s_t - s_{t-1} \|_2^2$ controls the smooth propagation within the same sequence, $\rho \sum_{(i,j)} y_{ij} \|\bar{s}_i - \bar{s}_j\|_2^2$ uses sample labels to constrain the discriminative structure between different patients or different states, $\bar{s}_i$ represents the sequence-level state representation, y_{ij} represents the sample relationship label, and ρ is the balance coefficient. This formula can reduce the random oscillation of the state vector in a short time, and avoid the excessive overlap of patients with different functional levels in the embedding space. Through the parallel optimization of smoothness constraint and discrimination constraint, the temporal representation layer obtains higher stability and clearer state boundary.

After this process, the knee joint function change no longer stays at the single point

judgment level, but is organized as a continuous state result that can reflect the action evolution process, which provides a direct basis for risk prediction.

3.4 Knee motion risk prediction module

The knee motion risk prediction module is built on the above functional state trajectory, and its goal is to output the risk probability according to the current state evolution trend, rather than simply review and judge the existing abnormalities. Elderly patients are prone to occult instability during gait transition, standing up, short-distance turning and weight-bearing movement. Such changes are not necessarily accompanied by obvious falls or pain in a short period of time, but will leave a cumulative shift in the state trajectory. Based on this characteristic, this paper adopts the probabilistic risk inference framework, which integrates functional state representation, stability index and individual baseline into the risk estimation process, so that the output result is not only statistically significant, but also retains the individual adaptation ability.

In order to transform the sequence-level state representation into the risk posterior probability, this paper first defines the underlying risk classification expression as follows.

$$P(r \mid \bar{s}) = \mathrm{Softmax}(W_r \bar{s} + b_r) \tag{10}$$

Here, $\bar{s}$ is the sequence-level functional state representation, W_r and b_r are risk classification parameters, and r represents the risk level category. The output of this formula is the initial risk distribution obtained based on the group training samples, which can reflect which type of risk state the patient's current action sequence is closer to in the overall sense. However, for elderly patients, the basic mobility, gait speed and knee range of motion vary greatly, and relying only on the unified classification boundary is prone to individual bias, so it is necessary to further introduce an individual threshold correction mechanism.

In order to enable the same model to adapt to patients with different basic mobility and different rehabilitation stages, this paper constructs an individualized risk threshold, which is calculated in the following equation.

$$\tau_i = \gamma_1 \bar{\kappa}_i + \gamma_2 \bar{\theta}_i^{-1} + \gamma_3 \bar{v}_i^{-1} \tag{11}$$

Here, τ_i is the individual risk threshold for the i patient, $\bar{\kappa}_i$ represents the average stability index, $\bar{\theta}_i$ represents the average flexion and extension range of motion, $\bar{v}_i$ represents the average gait speed, and γ_1 to γ_3 are the weight coefficients. The idea embodied in this equation is that patients with smaller range of motion, lower speed and greater fluctuation in stability should use more sensitive risk judgment boundaries. Through this correction process, the model can generate risk output with individual difference adaptation ability under a unified training framework, avoiding the mechanical classification of patients with low mobility into the high-risk category, and avoiding the insufficient response to early abnormalities in patients with high mobility.

To illustrate the way in which state representation, individual threshold and risk probability are connected, the risk module front-end computation chain is organized as Fig. 4 in this paper.

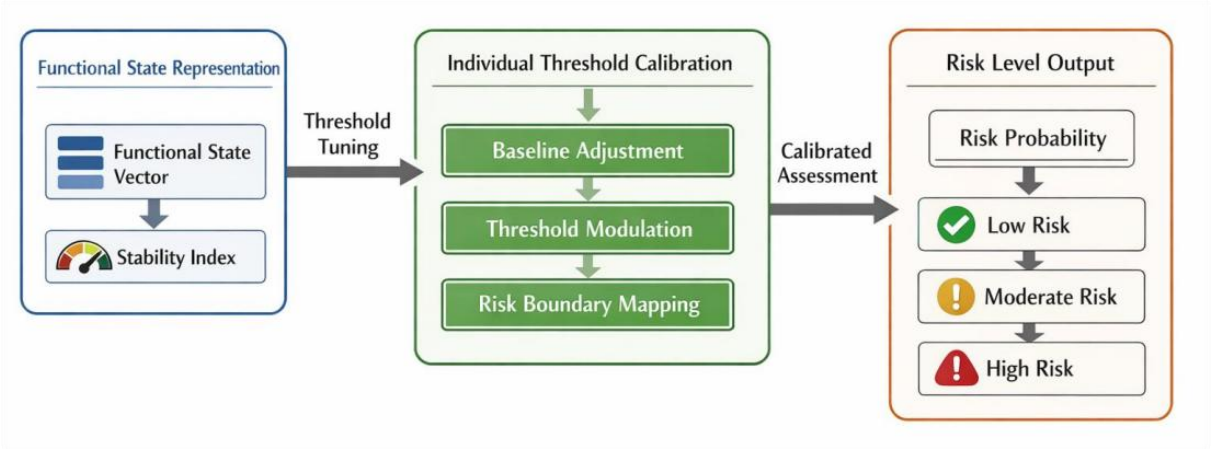

Figure 4: Inference flowchart for state input to risk score

Fig. 4 gives the complete path from sequence-level state representation to risk score generation. The left input is the functional state vector and stability index, the middle is the individual threshold correction layer, and the right is the risk level output layer. The flow firstly uses the state representation to restore the patient's functional level in the current action stage, and then adjusts the risk boundary combined with the individual baseline, and finally outputs the corrected risk probability. In this way, the risk results can reflect both group statistical characteristics and individual differences in exercise ability.

In order to incorporate the individual threshold and the underlying posterior probability into the unified decision, this paper introduces a Bayesian risk modification expression as follows.

$$P^*(r_i \mid \bar{s}_i, \tau_i) = \frac{P(r_i \mid \bar{s}_i) \cdot \exp(-|\hat{\kappa}_i - \tau_i|)}{\sum_c P(c \mid \bar{s}_i) \cdot \exp(-|\hat{\kappa}_i - \tau_i|)} \tag{12}$$

where $P^*(r_i \mid \bar{s}_i, \tau_i)$ is the corrected risk probability, $\hat{\kappa}_i$ is the estimated value of the current series stability index. This formula uses the distance between the individual threshold and the current state to reweight the original classification result. When the current stability index significantly exceeds the individual threshold, the high-risk posterior will be amplified. When the state fluctuation is still within the patient's tolerable range, the risk output will fall back accordingly. This allows the model to give more sensitive cues at early stages of fluctuations, while avoiding overreacting to normal state fluctuations.

In order to make the training stage take into account both classification accuracy and risk ranking ability, this paper defines the comprehensive loss function as follows.

$$\mathcal{L}_{\text{risk}} = \mathcal{L}_{\text{ce}} + \lambda_1 \mathcal{L}_{\text{rank}} + \lambda_2 \|p_{\text{high}} - p_{\text{low}}\|_2^{-1} \tag{13}$$

Here, $\mathcal{L}_{\text{ce}}$ represents the cross-entropy classification loss, $\mathcal{L}_{\text{rank}}$ represents the risk ranking loss, and p_{high} and p_{low} represent the posterior probability vectors of high-risk and low-risk samples, respectively. This formula not only ensures the correct classification, but also requires the high-risk samples to maintain a clearer interval from the low-risk samples in the probability space, so as to enhance the ability of the model to distinguish the boundary samples. For the elderly patient scenario, there are no extreme differences between many dangerous sequences and safe sequences, and the ordering constraint can improve the sensitivity of the model to subtle state shifts, so that the risk score is closer to the real action trend.

After individual threshold correction and probability posterior update, the model can convert the hidden instability trend in the continuous action sequence into a readable risk level result.

4 Experimental Evaluation

4.1 Experimental Design

In this study, the experimental design was carried out synchronously around the two tasks of intelligent assessment of knee function and movement risk prediction in elderly patients. In order to ensure the authenticity of data sources, stable labels and reproducible processes, all samples were obtained from outpatient rehabilitation assessment and standard movement test records. Informed consent and anonymization were completed before collection, and the patient's name, image identity information and medical record number were not entered into the training process. The final dataset contained 1240 valid samples from 186 elderly patients. Each sample consisted of gait video clips, inertial measurement sequences, plantar pressure matrix and knee flexion and extension Angle records, and the labels included function score level and movement risk level.

In order to reduce the offset caused by the difference in sampling frequency of different devices, the video stream was uniformly resampled to 25 fps, and the inertial signal and pressure sequence were aligned according to the timestamp and divided into a 50-frame window, and the step size was set to 25 frames. The function assessment task was double-labeled with continuous scoring and grading labels, and the risk prediction task was labeled with low, medium and high three-level labels, in which high-risk samples accounted for 28.6%, medium-risk samples accounted for 34.1%, and the rest were low-risk samples. In order to enhance the training stability, the model adopted a joint strategy of category weighting and stratified sampling. The main experimental data and training configuration are shown in Table 2.

Table 2: Experimental data with training configuration

Item	Setting
Number of Patients	186
Number of Samples	1240
Input Modalities	Video, IMU, plantar pressure, flexion-extension angle
Time Window	50 frames
Stride	25 frames
Training/Validation/Test Split	8:1:1
Optimizer	Adam
Initial Learning Rate	0.001
Batch Size	32
Number of Training Epochs	60
Hardware Environment	RTX 3090

The experimental group adopted the proposed model, and the control group was set as CNN-LSTM, random forest, and unimodal baseline models. CNN-LSTM was used to verify the modeling ability of the deep temporal network for continuous action clips, random forest was used to compare the performance of traditional machine learning under the condition of structured features, and the single-modal baseline model only retained video input or pressure

input, respectively, to test the performance gain brought by multimodal fusion. All samples were divided independently by patient, and the ratio of training set, validation set and test set was 8:1:1. The data of the same patient did not appear in different subsets at the same time to avoid high results caused by individual information leakage.

The model training was implemented by PyTorch, Adam was selected as the optimizer, the initial learning rate was set to 0.001, and the attenuation was 0.1 times every 20 rounds. The batch size was 32, and the maximum number of training rounds was 60. The function evaluation branch is jointly optimized by mean square error loss and rank cross entropy, and the risk prediction branch is jointly trained by weighted cross entropy and ranking loss. dropout of 0.4 is added after the main layer, and L2 regularization is used to suppress overfitting. The evaluation metrics include functional score mean absolute error, risk prediction accuracy, precision, recall, and F1-score. The whole experiment was completed on the RTX 3090 platform, and the experiment log, parameter file and data partition index were uniformly saved.

4.2 Experimental Results

In order to verify the comprehensive performance of the model in the intelligent assessment of knee function and movement risk prediction of elderly patients, the experimental results are analyzed from four levels: function scoring error, risk classification performance, multi-modal input adaptability and module contribution. All the results are obtained based on independent test sets and five-fold cross validation. The evaluation metrics include mean absolute error of functional score, risk prediction accuracy, precision, recall and F1-score.

In order to observe the error distribution of different models in the function scoring task, this paper first presents the box plot of scoring error of each model in the test set, as shown in Fig. 5.

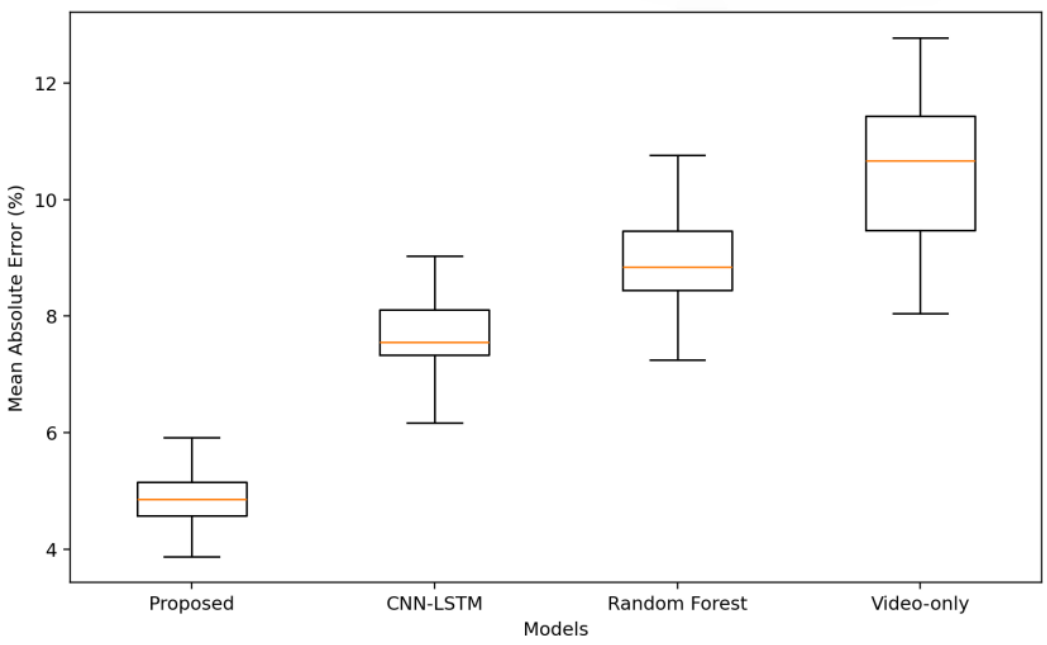

Figure 5: Box plots of knee function score error distribution for different models

As shown in Fig. 5, the error distribution of the proposed model is the most concentrated, with a median error of 4.7% and a mean absolute error of 4.9%, which are significantly lower

than 7.6% of the CNN-LSTM model, 9.1% of the random forest model, and 10.4% of the video unimodal model. At the same time, the box range of the proposed model is narrower and the number of outliers is smaller, which indicates that it maintains high stability among different patient samples. The results show that after multimodal feature fusion and temporal state representation work together, the model can more accurately recover the knee joint function change process, and reduce the fluctuation error common in traditional single-modal modeling.

In order to compare the comprehensive ability of different models in the motion risk prediction task, this paper further presents the radar chart composed of four main classification indicators, as shown in Fig. 6.

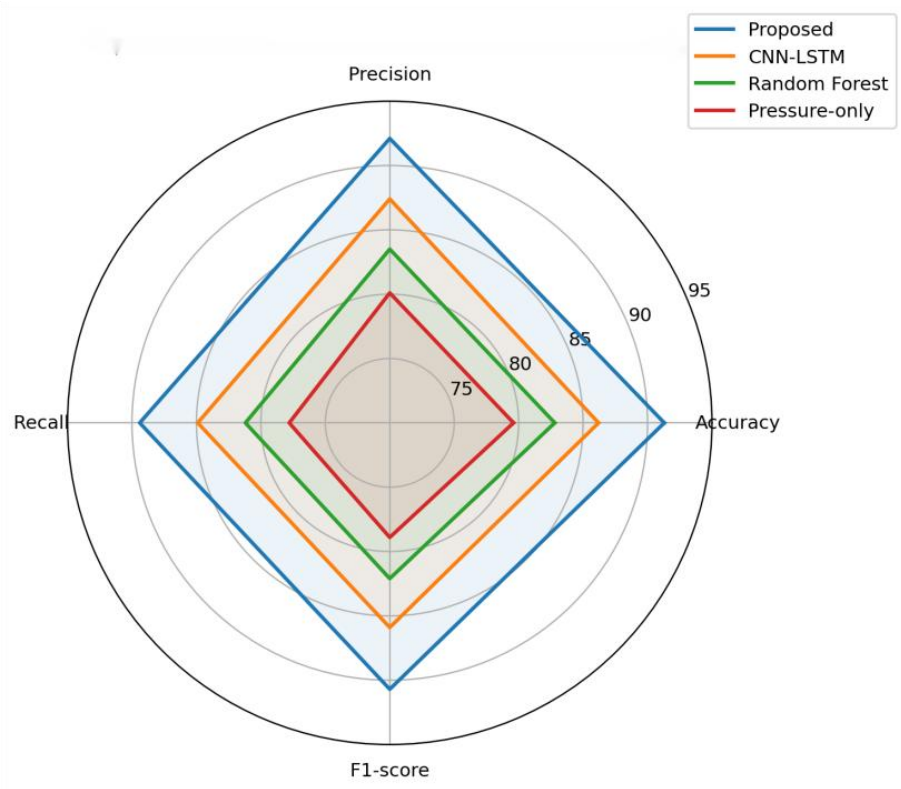

Figure 6: Radar plot of motion risk prediction performance of different models

Fig. 6 shows that the proposed model is in the outer edge position in the four indicators of accuracy, precision, recall and F1-score, and the risk prediction accuracy reaches 91.3%, the precision reaches 92.1%, the recall reaches 89.4%, and the F1-score reaches 90.7%. In comparison, the CNN-LSTM model achieves 86.2% accuracy, the random forest model achieves 82.8% accuracy, and the pressure unimodal model achieves 79.6% accuracy. This result shows that the model in this paper does not rely on the local improvement of a single index to obtain the overall advantage, but maintains a good balance between multiple indicators, so it has higher practical value in the knee joint risk assessment of elderly patients.

In order to more clearly compare the functional assessment and risk prediction results under different input combinations, the corresponding experimental results are organized in Table 3.

Table 3: Results of functional evaluation and risk prediction under different input combinations

Input Combination	Functional Score MAE (%)	Risk Accuracy (%)	F1-score (%)
Video + IMU + Pressure + Angle	4.9	91.3	90.7
Video + IMU + Pressure	5.6	88.4	87.9
Video + Pressure + Angle	5.8	87.6	86.8
IMU + Pressure + Angle	5.4	89.1	88.5
Video Only	10.4	78.7	77.9

Table 3 shows that the optimal results are achieved for the full multimodal input, and the performance decreases after missing either modality. Among them, the risk accuracy decreased by 2.9 percentage points after removing the Angle stream, and the function scoring error increased by 0.9 percentage points after removing the video stream. This indicates that visual trajectory information plays an obvious role in the recovery of action structure, while flexion and extension Angle flow and pressure matrix are more sensitive to risk level classification. Overall, the multimodal input not only improves the accuracy of the model, but also enhances the discrimination between different functional states.

In order to investigate the discrimination effect of the model in different risk levels, this paper presents the confusion matrix heatmap of three-level risk classification, as shown in Fig. 7.

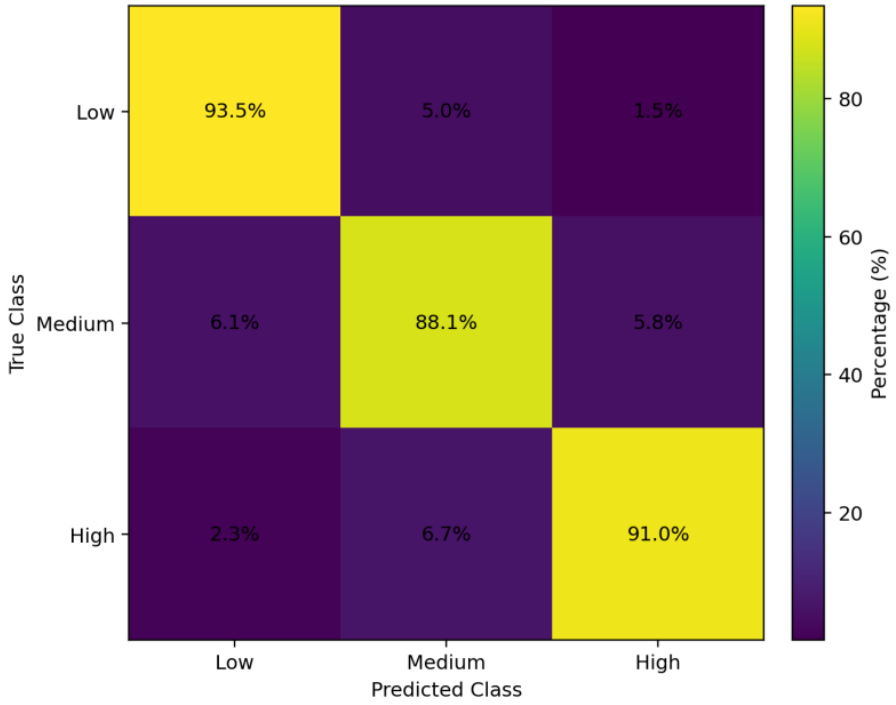

Figure 7: Heatmap of confusion matrix for three-level exercise risk classification

Fig. 7 indicates that the identification of low-risk versus high-risk samples is the most stable, and the diagonal region has the strongest response. Specifically, the recognition rate of low risk samples is 93.5%, the recognition rate of medium risk samples is 88.1% and the recognition rate of high risk samples is 91.0%. There is a small amount of transfer to adjacent

grades in the medium-risk samples, which indicates that the critical state interval still has a certain overlap, but the overall misclassification ratio remains at a low level. This result reflects that the proposed model can effectively identify stability fluctuations in continuous action clips and maintain a good discrimination boundary for different risk levels.

In order to verify the specific contribution of the internal structure of the model to the performance improvement, this paper sets up the ablation experiment separately, and the relevant results are listed in Table 4. This table is used to analyze the change in performance after module removal and does not repeat the previous inter-model comparison.

Table 4: Results of ablation experiments

Model Setting	Functional Score MAE (%)	Risk Accuracy (%)	F1-score (%)
Full Model	4.9	91.3	90.7
Without Multimodal Fusion	6.3	86.9	85.8
Without Temporal Representation	6.0	87.4	86.3
Without Probability Calibration	5.5	88.2	87.1

Table 4 shows that the model degradation is the most obvious after removing the multi-modal fusion, the functional scoring error increases to 6.3%, and the risk accuracy decreases to 86.9%. After removing the temporal representation, the recognition ability of the model for continuous action changes was weakened, and the F1-score decreased by 4.4 percentage points. After removing the probability correction, the balance between precision and recall becomes significantly worse. It can be seen that the three parts of multimodal fusion, temporal representation and probability correction assume different roles of input unification, state modeling and risk correction respectively in the proposed framework, and the lack of any one will weaken the overall performance.

In order to show the distribution characteristics and clustering status of the model in different test folds, this paper further presents the clustered scatter plot of the five-fold cross-validation results, as shown in Fig. 8.

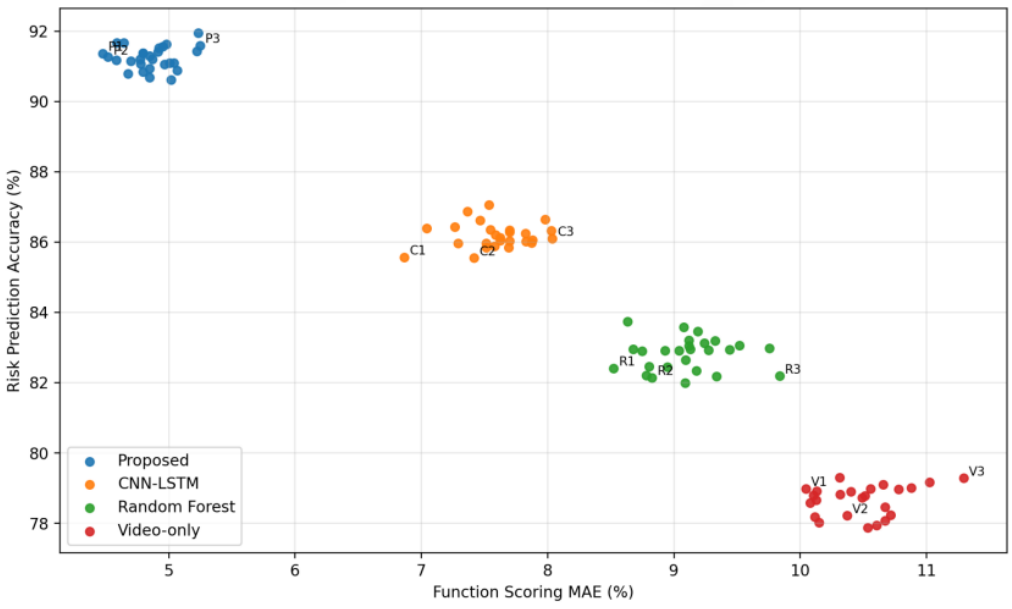

Figure 8: Clustered scatter plot of five-fold cross-validation results

Fig. 8 shows that different models form relatively clear distribution clusters in the two-dimensional space of function scoring error and risk prediction accuracy. The scatter points of the model in this paper are mainly concentrated in the region of functional scoring error 4.7% to 5.1% and risk prediction accuracy 90.6% to 91.9%. The degree of dispersion between points is small and the clustering boundary is tight, indicating that the model has good stability and consistency under different data partitions. In contrast, the scatter distributions of CNN-LSTM, random forest, and video unimodal models are more scattered, and the overall bias is toward regions of higher error and lower accuracy, indicating that they are more sensitive to test fold changes. The results show that the multimodal input and probability correction mechanism not only improve the overall performance of the model, but also enhance the concentration and repeatability of the result output under different cross-validation partition conditions.

In order to further judge whether the model performance improvement is statistically significant, this paper conducts a significance test on the main control methods, and the results are summarized in Table 5.

Table 5: Results of statistical tests between models

Compared Model	MAE Difference	Risk Accuracy Difference	p-value
CNN-LSTM	-2.7%	+5.1%	<0.01
Random Forest	-4.2%	+8.5%	<0.01
Video-Only Model	-5.5%	+12.6%	<0.01

Table 5 further illustrates that the performance improvement of the proposed model over each control method is statistically significant and not a chance result caused by the fluctuation of sample division. The decrease of function scoring error remains stable in different control groups, and the improvement of risk prediction accuracy also reaches a significant level, which indicates that the model in this paper has formed a more reliable advantage in both functional assessment accuracy and risk identification ability.

Synthesizing the above chart results, it can be confirmed that the proposed model is superior to the control methods in terms of functional scoring error control, risk classification balance, multi-modal adaptability and cross-validation stability. The experimental results are consistent with the core indicators in the abstract, which also shows that the framework can form stable, continuous, and interpretable computational output in the knee joint scene of elderly patients.

4.3 Experimental Discussion

The experimental results show that the proposed model has stable advantages in the two tasks of intelligent assessment of knee function and movement risk prediction in elderly patients. The mean absolute error of functional score is controlled at 4.9%, and the accuracy of risk prediction reaches 91.3%, which indicates that there is a close synergistic relationship between multi-modal fusion, temporal state representation and probability correction. Compared with CNN-LSTM, random forest and unimodal baselines, the improvement of the proposed model is not only reflected in a single indicator, but also reflected in smaller fluctuations in different test compromises and more concentrated output across patients. The reason is that the video trajectory, plantar pressure, inertial signal and flexion and extension Angle sequences complete the quality perception weighting in the fusion stage, and the local distortion input will not dominate the overall state expression. In the time series modeling phase, the phase attention and stability index can continuously capture the dynamic changes

such as support transition hysteresis, gait deceleration and load offset. In the risk determination stage, the individual threshold correction weakens the error caused by the uniform classification boundary. In the experiment, there is still a small amount of adjacent grade confusion in the medium-risk sample, indicating that the representation of critical state can be further refined, but the overall ranking relationship has been relatively clear. Combined with the training and inference costs, the current model has the application basis for outpatient screening, rehabilitation follow-up and home monitoring. In the actual deployment scenario, the framework can also form linkage with wearable acquisition terminals and edge computing nodes, so that continuous monitoring, status update and risk warning can maintain the same data link, so as to improve the real-time performance and consistency of result output.

5 Conclusion

This paper constructs an integrated computing framework around the intelligent assessment of knee function and motion risk prediction in elderly patients, and forms a collaborative design at three levels: multi-modal data fusion, temporal representation of functional status and probabilistic risk judgment. Experimental results show that the model achieves stable performance in functional scoring error control and risk level recognition, which indicates that video, pressure, inertia and Angle information can effectively complement each other in a unified state space. This framework provides a continuous and quantifiable technology path for outpatient screening, rehabilitation follow-up and home monitoring, and also provides a deployable basis for assistant decision-making in intelligent medical scenarios. It should also be noted that the current model has several limitations. The sample source focuses on elderly patients in a single center, the action scene is mainly based on standard assessment tasks, and the data distribution is still biased towards the controlled environment, which will limit the transfer stability of the model in complex family scenes. Multi-modal input improves the recognition accuracy, but the sampling error, wearing offset and local missing between different devices may still affect the consistency of state expression. The risk prediction part currently uses a three-level classification, which is suitable for clinical stratification and early warning output, but the description of the critical transition state can be further refined. Future research can be carried out from three directions: expanding multi-center samples and introducing richer daily action sequences to enhance the generalization ability of the model across people and scenes. Edge computing and lightweight network compression were combined to improve the efficiency of mobile terminal deployment. Self-supervised pre-training and individual long-term trajectory modeling were introduced to enable the system to learn patient change rhythms and form fine-grained and more continuous functional assessment and risk inference results.

Funding

This work was supported by Sichuan Provincial Natural Science Foundation (NO: 2024NSFSC0568)

References

[1] Ben Hassine S, Balti A, Abid S, et al. Markerless vision-based knee osteoarthritis classification using machine learning and gait videos[J]. Frontiers in Signal Processing, 2024, 4: 1479244.

[2] Xie J, Li S, Song Z, et al. Functional monitoring of patients with knee osteoarthritis based on multidimensional wearable plantar pressure features: Cross-Sectional study[J]. JMIR aging, 2024, 7(1): e58261.

[3] Li G, Li S, Xie J, et al. Identifying changes in dynamic plantar pressure associated with radiological knee osteoarthritis based on machine learning and wearable devices[J]. Journal of NeuroEngineering and Rehabilitation, 2024, 21(1): 45.

[4] Raza A, Sekiguchi Y, Yaguchi H, et al. Gait classification of knee osteoarthritis patients using shoe-embedded internal measurement units sensor[J]. Clinical Biomechanics, 2024, 117: 106285.

[5] Armstrong K, Zhang L, Wen Y, et al. A marker-less human motion analysis system for motion-based biomarker identification and quantification in knee disorders[J]. Frontiers in Digital Health, 2024, 6: 1324511.

[6] Zhao Z, Yang T, Qin C, et al. Exploring the potential of the sit-to-stand test for self-assessment of physical condition in advanced knee osteoarthritis patients using computer vision[J]. Frontiers in Public Health, 2024, 12: 1348236.

[7] Maiora J, Rezola-Pardo C, García G, et al. Older adult fall risk prediction with deep learning and timed up and go (TUG) test data[J]. Bioengineering, 2024, 11(10): 1000.

[8] Lim Z K, Connie T, Goh M K O, et al. Fall risk prediction using temporal gait features and machine learning approaches[J]. Frontiers in Artificial Intelligence, 2024, 7: 1425713.

[9] Nishiyama D, Arita S, Fukui D, et al. Accurate fall risk classification in elderly using one gait cycle data and machine learning[J]. Clinical biomechanics, 2024, 115: 106262.

[10] González-Castro A, Leirós-Rodríguez R, Prada-García C, et al. The applications of artificial intelligence for assessing fall risk: systematic review[J]. Journal of medical internet research, 2024, 26: e54934.

[11] Wipperman M F, Lin A Z, Gayvert K M, et al. Digital wearable insole-based identification of knee arthropathies and gait signatures using machine learning[J]. Elife, 2024, 13: e86132.

[12] Xu Z, Wu Z, Wang L, et al. Research on monitoring assistive devices for rehabilitation of movement disorders through multi-sensor analysis combined with deep learning[J]. Sensors, 2024, 24(13): 4273.

[13] Shen C, Pei Z, Chen W, et al. A wearable knee rehabilitation system based on graphene textile composite sensor: Implementation and validation[J]. Engineering Applications of Artificial Intelligence, 2024, 136: 108954.

[14] Hu R, Diao Y, Wang Y, et al. Effective evaluation of HGcnMLP method for markerless 3D pose estimation of musculoskeletal diseases patients based on smartphone monocular video[J]. Frontiers in Bioengineering and Biotechnology, 2024, 11: 1335251.

[15] Cedeno-Moreno R, Malagon-Barillas D L, Morales-Hernandez L A, et al. Computer

vision system based on the analysis of gait features for fall risk assessment in elderly people[J]. Applied Sciences, 2024, 14(9): 3867.

[16] Feng Y, Liu Y, Fang Y, et al. Advances in the application of wearable sensors for gait analysis after total knee arthroplasty: a systematic review[J]. Arthroplasty, 2023, 5(1): 49.

[17] Gianzina E, Kalinterakis G, Delis S, et al. Evaluation of gait recovery after total knee arthroplasty using wearable inertial sensors: A systematic review[J]. The Knee, 2023, 41: 190-203.

[18] Ceballos-Laita L, Marimon X, Masip-Alvarez A, et al. A beta version of an application based on computer vision for the assessment of knee valgus angle: a validity and reliability study[C]//Healthcare. MDPI, 2023, 11(9): 1258.

[19] Talaa S, El Fezazi M, Jilbab A, et al. Computer Vision-Based Approach for Automated Monitoring and Assessment of Gait Rehabilitation at Home[J]. International Journal of Online & Biomedical Engineering, 2023, 19(18).

[20] Horsak B, Eichmann A, Lauer K, et al. Concurrent validity of smartphone-based markerless motion capturing to quantify lower-limb joint kinematics in healthy and pathological gait[J]. Journal of Biomechanics, 2023, 159: 111801.

[21] Iovanel G, Ayers D, Zheng H. The role of wearable technology in measuring and supporting patient outcomes following total joint replacement: review of the literature[J]. JMIR Perioperative Medicine, 2023, 6(1): e39396.